CHEMISTRY OF MATERIALS

Article

pubs.acs.org/cm

Effects of Functionalized Gold Nanoparticle Size on X-ray Attenuation and Substrate Binding Affinity

Ryan D. Ross,[†] Lisa E. Cole, Jennifer M. R. Tilley, and Ryan K. Roeder*

Department of Aerospace and Mechanical Engineering, Bioengineering Graduate Program, University of Notre Dame, Notre Dame, Indiana 46556, United States

Supporting Information

ABSTRACT: Gold nanoparticles (Au NPs) have attracted interest as an X-ray contrast agent due to exhibiting high X-ray attenuation, colloidal stability, vascular retention, and facile surface functionalization for targeted delivery to cells and tissues. However, the effects of Au NP size on X-ray attenuation and binding affinity to a targeted surface are not well-understood. Therefore, the effect of Au NP size on X-ray attenuation was investigated by preparing mercaptosuccinic acid functionalized Au NPs exhibiting a mean particle diameter of 5, 13, 35, or 76 nm, as well as chloroauric acid control, at gold concentrations up to ~50 mM (~10 g/L). The X-ray attenuation of Au NP and chloroauric acid solutions increased with decreased photon energy and increased linearly with increased gold concentration, but was independent of the particle diameter. The effects of Au NP size on substrate binding affinity were investigated by preparing bisphosphonate functionalized Au NPs exhibiting a mean particle diameter of 5, 13, 35, or 76 nm and measuring binding isotherms using hydroxyapatite (HA) crystals as a model for bone mineral or microcalcifications. Decreased Au NP diameter resulted in an increased number of Au NPs but decreased mass of gold adsorbed onto HA crystal surfaces, and thus a lower binding affinity to HA. Therefore, the results of this study suggest that for targeted labeling of HA, or calcified tissue, an increased Au NP diameter will improve detection due to a greater of mass of gold labeling surfaces and thus greater X-ray attenuation.

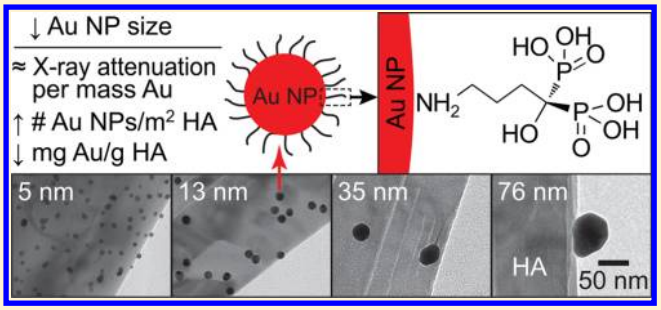

KEYWORDS: *gold nanoparticles, contrast agent, X-ray attenuation, hydroxyapatite, binding affinity, bisphosphonate, targeted delivery*

INTRODUCTION

Contrast agents have been used since the discovery of X-rays to enhance the X-ray attenuation of soft tissues and organs for radiographic imaging.[1] Current clinical applications primarily include gastrointestinal imaging using barium sulfate suspensions and vascular imaging using iodinated molecular agents. The potential of gold nanoparticles (Au NPs) as an X-ray contrast agent was first reported by Hainfeld et al.[2,3] Au NPs have subsequently received considerable recent interest as a vascular contrast agent due to exhibiting greater X-ray attenuation per mass compared to iodinated molecular agents, such as iohexol,[3−7] iopromide,[8,9] and iopamidal,[10,11] although the extent of improvement is dependent on imaging parameters.[9,10] Perhaps more importantly, properly stabilized Au NPs have also exhibited improved vascular retention compared to iodinated molecules[3,4,8] and are nontoxic,[12−14] which could extend the available time-window for clinical imaging and enable targeted delivery in vivo.

The high specific surface area and surface chemistry of Au NPs are amenable to surface functionalization via thiol, amine, and phosphine linkages to molecules providing various ligands for targeting cells and tissues or to other molecular contrast agents for multimodal imaging. Thus, Au NPs have been surface functionalized with antibodies,[15−17] peptides,[18,19] and monosaccharides[20] for targeting cancerous cells,[15,17−20] cancerous tissue,[17,18] and lymph nodes[16] to provide enhanced contrast for detection by computed tomography (CT) both in vitro[15,17,19,20] and in vivo.[16−18] Au NPs surface functionalized with carboxylate and bisphosphonate ligands exhibit binding affinity for hydroxyapatite (HA) and have thus been investigated for targeting calcified tissue, for example, to label microdamage in bone tissue[21−23] or breast microcalcifications.[24] Au NPs surface functionalized with gadolinium chelates have been investigated as a multimodal contrast agent for magnetic resonance imaging.[25,26]

The effects of Au NP size and morphology on optical properties (e.g., surface plasmon resonance) are well-known,[27−29] but conflicting data have been reported for the effects of Au NP size on X-ray attenuation. Mercaptosuccinic acid (MSA) stabilized Au NPs were reported to exhibit increased X-ray attenuation with decreased particle diameter, for a mean particle diameter of 4, 20, 40, and 60 nm and gold concentrations up to 30 mM (~6 g/L), using CT at 120 kVp and 625 μm resolution.[5] In contrast, a more recent study reported that X-ray attenuation was affected by neither size nor

Received: October 28, 2013
Published: December 19, 2013

shape for Au NPs exhibiting a mean particle diameter of 4, 6, and 25 nm, as well as 30 × 60 nm Au nanorods, at a gold concentration of 5 g/L (~25 mM) using radiography at X-ray photon energies of 40, 60, 80, or 100 kVp and ~150 μm resolution.[6]

The size of functionalized Au NPs could also indirectly affect X-ray attenuation after targeted delivery through size-dependent differences in binding affinity, colloidal stability, biotransport, or endocytosis. For example, the X-ray attenuation of lymph nodes targeted by antibody functionalized Au NPs was greater for a larger particle diameter.[16] The effects of functionalized Au NP size on colloidal stability,[30,31] biotransport,[31−34] and endocytosis[35−38] have been reported,[39] but investigations of the effects on binding affinity are lacking. The binding affinity of antibody functionalized Au NPs to a cell receptor increased by more than 1 order of magnitude for a 7-fold increase in particle diameter and was attributed to an increased surface density of functional groups with increased nanoparticle size.[36] However, the study of binding affinity to cells is complicated by cell signaling and endocytosis.

Therefore, the objective of this study was to investigate the effects of functionalized Au NP size on (1) X-ray attenuation and (2) binding affinity to HA crystals. The effect of size on X-ray attenuation was investigated by preparing MSA functionalized Au NP solutions exhibiting a mean particle diameter of 5, 13, 35, or 76 nm, as well as a chloroauric acid control, at gold concentrations up to ~50 mM (~10 g/L), which constituted a wider range in size and concentration than the previous studies reporting conflicting results.[5,6] Moreover, X-ray attenuation was measured at higher resolution and two energy levels using micro-computed tomography (micro-CT). The effect of Au NP size on binding affinity was investigated by preparing bisphosphonate functionalized Au NPs exhibiting a mean particle diameter of 5, 13, 35, or 76 nm and measuring binding isotherms using a clinically relevant and highly reproducible in vitro model system comprising HA as a synthetic analogue of bone mineral or breast microcalcifications.

EXPERIMENTAL METHODS

Au NP Synthesis. Gold nanoparticles (Au NPs) were synthesized with a mean diameter of 5, 13, 35, or 76 nm. Au NPs with a mean diameter of 13 nm were prepared using the citrate reduction method, as described in detail elsewhere,[22,23] and larger diameter Au NPs were prepared by adjusting the gold to citrate ratio.[40] In each case, 0.1 g of chloroauric acid ($HAuCl_4 \cdot 3H_2O$, ≥99.9%, Sigma-Aldrich, St. Louis, MO) was added to 400 mL of DI water and brought to a boil while stirring. Trisodium citrate dihydrate (ACS reagent, >99%, Sigma-Aldrich) was added in an amount dependent on the desired particle diameter: 0.5 g for 13 nm, 0.1 g for 35 nm, and 0.08 g for 76 nm Au NPs. After the sodium citrate reducing agent was added, the mixture was allowed to boil for an additional 20 min before removing heat and stirring overnight. Au NPs with a mean diameter of 5 nm were prepared using a modified method.[41] 1.7 mL of a 1 wt % aqueous solution of $HAuCl_4$ was added to 80 mL of DI water under stirring. A reducing solution was prepared by mixing 6.8 mL of 1 wt % sodium citrate, 5.95 mL of 1 wt % tannic acid (ACS reagent, Sigma-Aldrich), and 5.95 mL of 25 mM K_2CO_3 (ACS reagent, >99%, Sigma-Aldrich). The $HAuCl_4$ and reducing solutions were both heated to 60 °C before adding the reducing solution to the $HAuCl_4$ solution and heating the combined solution to a boil. After 10 min of vigorous boiling, 6.7 mL of 30 wt % H_2O_2 (ACS reagent, Sigma-Aldrich) was added, and the solution was boiled for an additional 5 min before removing heat and stirring the colloidal gold dispersion overnight. Regardless of particle diameter, all Au NP solutions were prepared to a gold concentration of 0.5 mM (~0.1 g/L).

Au NP Surface Functionalization. Au NPs were prepared for surface functionalization by removing excess ions from the synthesis. Ten milliliters of 2 wt % polyvinyl alcohol (PVA 10-98, M_w = 61 000 Da, Fluka, St. Louis, MO) was added to 240 mL of as-prepared Au NP solutions, followed by 6.0, 5.8, 5.0, or 1.5 g of ion-exchange resin (Amberlite MB-150, Sigma-Aldrich) for Au NPs with a mean diameter of 5, 13, 35, or 76 nm, respectively. These solutions were stirred overnight and subsequently filtered (grade 3, Whatman, Piscataway, NJ) to remove the ion-exchange resin. For X-ray attenuation measurements, Au NPs were surface functionalized with mercaptosuccinic acid (MSA, 97%, Sigma-Aldrich) to maintain colloidal stability. 4.1, 4.0, 3.6, or 2.0 mL of a 0.01 M solution of MSA was added to 240 mL of as-prepared Au NP solutions comprising Au NPs with a mean diameter of 5, 13, 35, or 76 nm, respectively. For binding experiments, Au NPs were surface functionalized with alendronate sodium trihydrate (≥97%, Sigma-Aldrich), a bisphosphonate, using the same solution volumes and concentrations as for MSA. Note that Au NPs were exposed to an excess of either MSA or bisphosphonate molecules to maximize surface coverage. After bisphosphonate functionalization, excess functional molecules were removed by dialysis (Spectra/Por, MWCO = 3500 Da, Spectrum Laboratories, Rancho Dominquez, CA) against DI water over 4 d, changing the water solution at least twice daily. Bisphosphonate surface functionalization on 13 nm Au NPs was previously verified by Fourier-transform infrared spectroscopy and mass spectroscopy.[22]

The surface density of bisphosphonate molecules on Au NPs of each particle diameter was determined from the mass ratio of phosphorus to gold measured by inductively coupled plasma-optical emission spectroscopy (ICP-OES, Optima 8000, PerkinElmer, Waltham, MA), using similar methods as described in detail elsewhere.[42] Prior to dialysis, 8 mL aliquots of bisphosphonate functionalized Au NP solutions were washed five times with DI water using centrifugal filter units (Amicon Ultra-15, EMD Millipore Corp., Billerica, MA) at 4000 rpm for 30 min to remove unbound bisphosphonate molecules. Washed Au NP solutions were then acidified in ~3% v/v aqua regia (3:1 HCl to HNO_3) prior to analysis. Aqua regia was used to solubilize Au NPs and prevent coagulation at low pH. Calibration curves were created by diluting certified standard gold and phosphorus solutions (SPEX CertiPrep, Metuchen, NJ). The surface density of bisphosphonate molecules on Au NPs (#/nm^2) was calculated from the measured mass ratio of phosphorus to gold and the particle size distributions measured as described below, assuming prolate spheroids, a phosphorus to bisphosphonate molar ratio of 2:1, and a bulk density of gold of 19.3 g/cm^3.

Au NP Size and Morphology. The mean particle diameter, particle size distribution, and morphology of Au NPs were characterized using transmission electron microscopy (TEM, FEI Titan 80-300, Hillsboro, OR) at 80 kV accelerating voltage. TEM specimens were prepared by dropping a solution of MSA functionalized Au NPs onto carbon-coated grids and evaporating the solvent. The particle diameter and aspect ratio were measured for a total of 200 particles from two separate batches for each particle size as the mean and ratio, respectively, of the prolate and equatorial diameter of a prolate spheroid. The particle surface area was calculated as:

$$A = 2\pi a^2\left(1 + \frac{b}{a \cdot e}\sin^{-1}(e)\right), \quad e^2 = 1 - \frac{a^2}{b^2} \tag{1}$$

where a is the prolate diameter, b is the equatorial diameter, and e is the eccentricity of the prolate spheroid.

Ultraviolet−visible (UV−vis) spectra (Nanodrop 2000c, Thermo Scientific, Wilmington, DE) were collected for as-prepared bisphosphonate functionalized Au NP solutions at a constant gold concentration of 0.5 mM (~0.1 g/L). The surface plasmon resonance (SPR) peak was determined by the wavelength at the maximum absorbance for solutions comprising Au NPs with a mean diameter of 5, 13, 35, or 76 nm.

Effects of Au NP Size on X-ray Attenuation. Au NP solutions were concentrated by centrifugation (model 5418, Eppendorf, Hauppauge, NY), varying the rotor speed and duration to obtain Au

dx.doi.org/10.1021/cm4035616 | Chem. Mater. 2014, 26, 1187−1194

NP solutions of varying gold concentration ranging ~0.4 to 54 mM (~0.07 to 10.6 g/L). Chloroauric acid ($HAuCl_4 \cdot 3H_2O$, ≥99.9%, Sigma-Aldrich) solutions were also prepared in DI water at varying gold concentrations ranging from ~5.4 to 48 mM (~1.1 to 9.5 mg/L) and used as a control. Gold concentrations were measured using ICP-OES (Optima 7000, PerkinElmer), as described above.

Au NP solutions were imaged by micro-CT (μCT-80, Scanco Medical AG, Brüttisellen, Switzerland) at 800 ms integration time, 10 μm isotropic resolution, and two energy levels: 45 kVp at 177 μA and 70 kVp at 113 μA. The standard 0.5 mm aluminum filter was removed to increase the number of low energy photons in the beam. A 1 mL sample of Au NPs for each concentration and particle diameter was added to a polyethylene specimen tube (14 mm inner diameter, 16.7 mm outer diameter) and ultrasonically dispersed as a precaution to ensure uniform dispersion in solutions containing larger particle diameters. The Au NP solution and a second, identical tube containing only DI water were stacked vertically in the micro-CT specimen holder with respect to the axis of specimen rotation. Ten image slices were sampled from the Au NP solution, the DI water sample, and air in the tube above the solution, corresponding to a 22.7 μL sampling volume. The measured mean linear attenuation coefficient (μ) of Au NP solutions was converted to Hounsfield units (HU) using an internal sample calibration with the mean linear attenuation coefficients measured for air (−1000 HU) and water (0 HU). This internal calibration ensured that the measured attenuation of Au NP solutions was not influenced by X-ray source or detector fluctuations.

The X-ray attenuation of Au NP solutions was reported in HU as the mean (±standard deviation) for a total of five separate samples for each Au NP diameter and concentration and was plotted as a function of gold concentration for each particle size. The effects of the X-ray photon energy, gold concentration, particle diameter, and their interactions on the measured X-ray attenuation were examined by multivariate analysis of variance using a generalized linear model (GLM) with an exponential distribution to account for a non-normal distribution of data (JMP 10, SAS Institute Inc., Cary, NC). X-ray attenuation versus gold concentration was also fit for pooled data using linear least-squares regression. The level of significance for all tests was set at $p < 0.05$.

Effects of Au NP Size on Binding Affinity to HA. The binding affinity of bisphosphonate functionalized Au NPs of varying particle diameter to bone mineral was measured using HA crystals as a synthetic analogue. Calcium-deficient single crystal HA whiskers were prepared using the chelate decomposition method, as described in detail elsewhere.[43] As-prepared HA whiskers exhibited a mean length of ~18 μm and a mean width of ~2 μm.[43] The specific surface area of the HA crystals was 5.63 m^2/g as measured by Brunauer–Emmett–Teller (BET) N_2 absorption (Autosorb-1, Quantachrome Instruments, Boynton Beach, FL).[22]

Binding affinity tests were performed in triplicate for each Au NP diameter and concentration using previously established methods.[22] Briefly, 10 ± 0.1 mg HA crystals were added to bisphosphonate functionalized Au NP solutions of varying concentration for a fixed total solution volume of 15 mL. Bisphosphonate functionalized Au NP solutions were incubated with the HA crystals for 4 h at ambient temperature on a test tube rotator to allow binding. HA crystals and bound Au NPs were then separated from unbound Au NPs remaining in the supernatant solutions by centrifugation for 2 min at ~700g for 5, 13, and 35 nm Au NPs, or 1 min at ~350g for 76 nm Au NPs. The gold concentration in control and supernatant solutions, and the calcium concentration in supernatant solutions, was measured by ICP-OES, using the methods described above, to measure the amount of gold bound to HA crystals and verify the removal of HA crystals from the supernatant solution, respectively. Binding of bisphosphonate functionalized Au NPs to HA crystal surfaces was verified by TEM at 80 kV accelerating voltage after dispersing the collected HA crystals onto carbon-coated grids.

Binding isotherms were plotted as the mean (±standard deviation) amount of gold bound per mass of HA crystals added, V (mg Au/g HA), versus the initial gold concentration, $[S]$ (mg Au/L). Binding isotherms were modeled using the Langmuir–Freundlich (LF) isotherm:

$$V = \frac{V_{max}(k\cdot[S])^b}{1 + (K\cdot[S])^b} \quad (2)$$

where V is the amount of functionalized Au NPs bound per mass of HA crystals (mg/g), V_{max} is the maximum surface binding (mg/g), $[S]$ is the initial concentration of gold (mg/L), K is the equilibrium binding constant (L/mg), and b is the heterogeneity constant.[44] When $b = 1$, the LF equation reduces to the Langmuir isotherm, and deviation from unity characterizes deviation from Langmuir assumptions. K, V_{max}, and b were measured using nonlinear least-squares regression.[44] The maximum surface binding of functionalized Au NPs on HA crystals, V_{max} (mg Au/g HA), was also normalized to the specific surface area of HA crystals, V_{max}* (mg Au/m^2 HA), and calculated as the maximum number of Au NPs bound per surface area of HA crystals, V_{max}# (#/μm^2 HA). The number and surface area of Au NPs were estimated from the bulk density of gold (19.3 g/cm^3) and the measured mean particle dimensions.

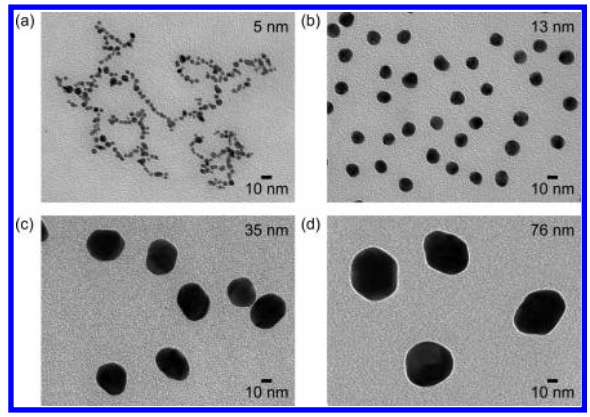

Figure 1. Representative TEM micrographs showing MSA functionalized Au NPs with a mean diameter of (a) 5, (b) 13, (c) 35, and (d) 76 nm. Particle diameter and aspect ratio measurements are summarized in Table 1, and particle diameter distributions are available as Supporting Information.

RESULTS AND DISCUSSION

Au NP Preparation and Characterization. Au NPs of varying mean particle diameter (Figure 1) were prepared by adjusting the ratio of the gold precursor salt to the citrate-based reducing agents. Au NPs with mean diameter of 5 and 13 nm were spherical and monodispersed; further increases in the mean particle diameter to 35 and 76 nm resulted in a slightly greater aspect ratio and a broader size distribution (Figure 1, Table 1). Increased heterogeneity of Au NPs with increased

Table 1. Mean (±standard deviation) Particle Diameter, Aspect Ratio, and Specific Surface Area of Functionalized Au NPs, and the Surface Density of Bisphosphonate Molecules on Au NP Surfaces[a]

particle diameter (nm)	aspect ratio	specific surface area (m^2/g)	BP surface density (#/nm^2)
4.7 (1.2)	1.2 (0.2)	72.9 (18.7)	1.2 (0.3)
13.2 (0.9)	1.1 (0.1)	24.3 (1.7)	3.5 (0.3)
35.0 (7.2)	1.3 (0.2)	9.8 (2.0)	20.2 (4.0)
76.4 (14.1)	1.5 (0.5)	4.8 (1.1)	11.1 (2.2)

[a]Particle diameter distributions are available as Supporting Information.

dx.doi.org/10.1021/cm4035616 | Chem. Mater. 2014, 26, 1187–1194

particle diameter was attributed to particle destabilization and has been previously reported for both gold and silver nanoparticles prepared using the citrate reduction method.[45,46] Au NPs with decreased diameter provided a greater specific surface area (Table 1) for scattering electromagnetic radiation (e.g., visible light or X-ray) and surface adsorption processes, including both functionalization and targeted delivery.

The surface density of bisphosphonate molecules on Au NP surfaces was nearly an order of magnitude greater for Au NPs with a mean diameter of 35 and 76 nm compared to Au NPs with a mean diameter of 5 and 13 nm (Table 1), as measured by ICP-OES. Decreased bisphosphonate surface density on NPs would be expected with increased specific surface area (or decreased particle diameter) for a fixed concentration of available bisphosphonate. However, Au NPs of each particle diameter were exposed to a greater than 10-fold excess of bisphosphonate molecules relative to the amount that bound to Au NP surfaces. Therefore, the measured differences in surface binding may also reflect differences in maximum binding, possibly due to differences in surface curvature.[47] Note that relatively few studies have quantitatively measured ligand surface density on Au NPs. A recent study that also used ICP-OES measured a size-independent surface density of ~8 molecules/nm^2 for a short alkanethiol on Au NPs over a similar size range as this study.[42] The results of the present study were comparable in magnitude, but lower for 5 and 13 nm diameter NPs and greater for 35 nm diameter NPs. The trends in the present study were also verified by measuring the unbound bisphosphonate concentrations in the supernatant wash solutions.

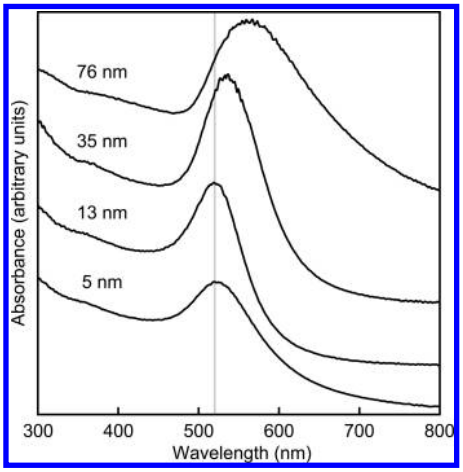

Figure 2. UV–vis spectra for as-prepared bisphosphonate functionalized Au NPs with a mean diameter of 5, 13, 35, and 76 nm dispersed in DI water at a gold concentration of 0.5 mM (~0.1 g/L) showing a red shift in the SPR peak with increased particle diameter. The SPR peak was located at 519, 519, 537, and 559 nm for Au NPs with a mean diameter of 5, 13, 35, and 76 nm, respectively. A gray reference line is shown at 520 nm for comparison.

UV–vis spectra of as-prepared functionalized Au NP solutions exhibited surface plasmon resonance (SPR) peaks at 519, 519, 537, and 559 nm, for Au NPs with a mean diameter of 5, 13, 35, and 76 nm, respectively (Figure 2). A red shift in the SPR peak with increased Au NP diameter was expected on the basis of the well-known size-dependence for absorption and scattering of visible light.[27−29] UV–vis spectra also indicated that Au NP solutions were well-dispersed. The SPR peak for 13 nm diameter bisphosphonate functionalized Au NPs was previously reported to remain unchanged for up to 7 days in deionized (DI) water, phosphate buffered saline, and fetal bovine serum, indicating colloidal stability.[23] While the effect of the Au NP diameter on colloidal stability was not explicitly investigated in this study, functionalized Au NPs with a mean diameter of 76 nm diameter were observed to become unstable in DI water after 2 days, which was consistent with previous studies demonstrating decreased stability with increased particle diameter.[30,31] Therefore, all X-ray attenuation and binding affinity measurements were performed within one day of preparation to ensure colloidal stability.

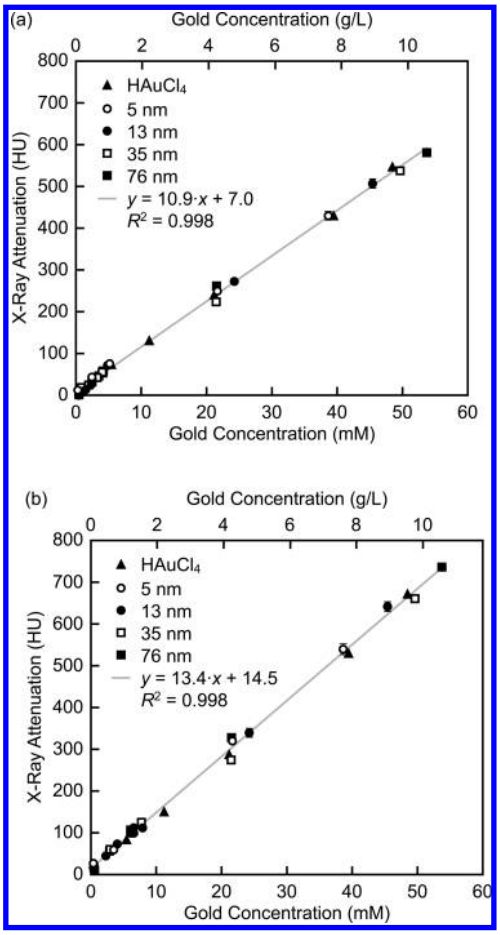

Figure 3. The mean linear attenuation coefficient measured by micro-CT at (a) 70 kVp and (b) 45 kVp for chloroauric acid ($HAuCl_4$) and MSA functionalized Au NPs with a mean diameter of 5, 13, 35, and 76 nm dispersed in DI water at gold concentrations ranging from ~0 to 54 mM (~0 to 10.6 g/L). Error bars show one standard deviation of the mean (n = 5 per data point). Error bars not shown lie within the data point. The effects of the group (particle diameter) and interaction (slope) were not statistically significant (p > 0.85, GLM). Therefore, least-squares linear regression of the pooled data is shown.

Effects of Au NP Size on X-ray Attenuation. The X-ray attenuation of Au NP and chloroauric acid ($HAuCl_4$) solutions increased linearly with gold concentration (p < 0.0001, generalized linear model, GLM), as expected (Figure 3). Differences between Au NPs with a mean diameter of 5, 13, 35, and 76 nm, and chloroauric acid solutions, as well as the interaction with gold concentration (slope), were not statistically significant (p > 0.85, GLM). Therefore, the pooled data

dx.doi.org/10.1021/cm4035616 | Chem. Mater. 2014, 26, 1187−1194

were fit by least-squares linear regression (Figure 3) and exhibited a strong correlation coefficient (R^2 = 0.998). Au NP and chloroauric acid solutions imaged at 45 kVp exhibited greater X-ray attenuation compared to 70 kVp ($p < 0.0001$, GLM), as expected (Figure 3). X-ray attenuation increases with decreased photon energy for any material, unless an absorption edge is encountered, due to a greater probability of photoelectric absorption with decreased photon penetration.[48−51]

The results of this study demonstrated that Au NPs with a mean particle diameter of 5, 13, 35, and 76 nm exhibited size-dependent optical properties (Figure 2), as expected,[27−29] but X-ray attenuation was not influenced by the Au NP diameter (Figure 3). Furthermore, the X-ray attenuation of aqueous solutions of chloroauric acid, comprising gold ions with atomic-scale dimensions, was also not different from aqueous dispersions of Au NPs. Previous studies reported conflicting results for the effect of Au NP size on X-ray attenuation.[5,6] The results of the present study carry greater significance as compared to both previous studies due to investigating a wider range of Au NP diameters and concentrations, including a chloroauric acid control group, verifying gold concentrations using ICP-OES, and imaging at higher resolution (10 μm) using micro-CT.

Previous reports of increased X-ray attenuation with decreased nanoparticle diameter must be called in question.[5,52] At the photon energy levels used in radiography and computed tomography (∼10−100 keV), the X-ray attenuation of high atomic number elements is governed by photoelectric absorption due to differences in mass concentration, while scattering processes, which could be partially influenced by differences in specific surface area, are insignificant in comparison.[48−51] Thus, the results of the present study confirmed no measurable effect of nanoparticle size on X-ray attenuation in X-ray absorption imaging systems. Similar results were also simultaneously confirmed in our laboratory for barium sulfate nanoparticles.[53]

The increased X-ray attenuation with decreased Au NP diameter reported in a previous study[5] could be attributed to several factors. X-ray attenuation measurements exhibited substantial variability, but no tests were performed to consider whether the measured differences were statistically significant. The reason for the relatively high variability in X-ray attenuation was not clear, but suggests colloidal instability. If Au NP solutions comprising larger particle diameters were less stable, larger diameter Au NPs and higher concentrations would be expected to exhibit artificially low X-ray attenuation and high variability. Therefore, the reported effect of nanoparticle size on radiographic contrast could not have been due to the physical effects of nanoparticle size, but was likely due to concomitant differences in dispersion and thus mass concentration.

Finally, the results of this study confirmed that the sensitivity for detecting cells or tissue labeled by Au NPs using X-ray absorption imaging techniques can only be feasibly improved by increasing the concentration of Au NPs, not by decreasing the particle diameter for a given concentration. However, decreased particle diameter could result in the delivery and/or binding of a greater concentration of Au NPs to the targeted cells or tissue. Therefore, the effect of the particle diameter on binding affinity was also investigated by measuring binding isotherms for bisphosphonate functionalized Au NPs to HA crystals with relatively flat surfaces and a large number of potential binding sites.

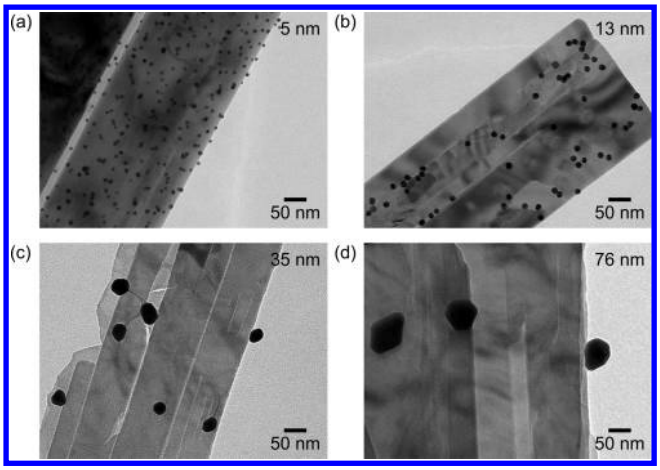

Figure 4. Representative TEM micrographs showing bisphosphonate functionalized Au NPs with a mean diameter of (a) 5, (b) 13, (c) 35, and (d) 76 nm adsorbed onto HA crystal surfaces after 4 h incubation in solutions containing Au NPs dispersed in DI water at ∼10 mg/L.

Effects of Au NP Size on Binding Affinity to HA. Binding of bisphosphonate functionalized Au NPs with a mean diameter of 5, 13, 35, and 76 nm to HA crystal surfaces was first confirmed by direct observation in TEM (Figure 4). The number of Au NPs bound to HA crystal surfaces increased with decreased Au NP diameter. However, for a fixed concentration, a greater number of smaller diameter Au NPs were initially available for binding regardless of the binding affinity. Therefore, binding isotherms were measured to enable quantitative comparisons based on Au NP mass or number, and per HA mass or surface area.

Binding isotherms for bisphosphonate functionalized Au NPs deviated from Langmuir assumptions with increased particle diameter but were accurately modeled by the Langmuir−Freundlich isotherm (Figure 5) with correlation coefficients exceeding 0.98 (Table 2). The heterogeneity constant, b, was close to unity at the smallest particle diameter, suggesting that the adsorption behavior did not deviate significantly from Langmuir equilibrium conditions (Table 2). However, heterogeneity increased with increased particle diameter (Table 2), most likely due to increased variability in the particle diameter and aspect ratio with increased particle diameter (Table 1).

Au NPs with a larger mean diameter exhibited greater binding affinity to HA, as evidenced by a greater amount of gold bound to HA on a per mass basis (mg/g) and a greater saturation concentration (Figure 5). Thus, increased Au NP diameter resulted in an increased equilibrium binding constant, K, and increased maximum surface binding per HA mass, V_{max}, or surface area, V_{max}* (Table 2). However, when converted to the number of Au NPs per HA surface area, the maximum surface binding, $V_{max}^{\#}$, decreased with increased particle diameter (Table 2), in agreement with TEM observations (Figure 4). Therefore, decreased Au NP diameter resulted in an increased number of Au NPs, but decreased mass of gold, adsorbed onto HA crystal surfaces.

Bisphosphonate functionalized Au NPs exhibited a relatively high equilibrium binding constant, K, and maximum surface binding, V_{max}, regardless of the nanoparticle diameter, suggesting a high affinity to HA surfaces. Bisphosphonate functionalized Au NPs were previously reported to exhibit a 6- and 16-fold greater binding affinity to HA compared to

dx.doi.org/10.1021/cm4035616 | Chem. Mater. 2014, 26, 1187−1194

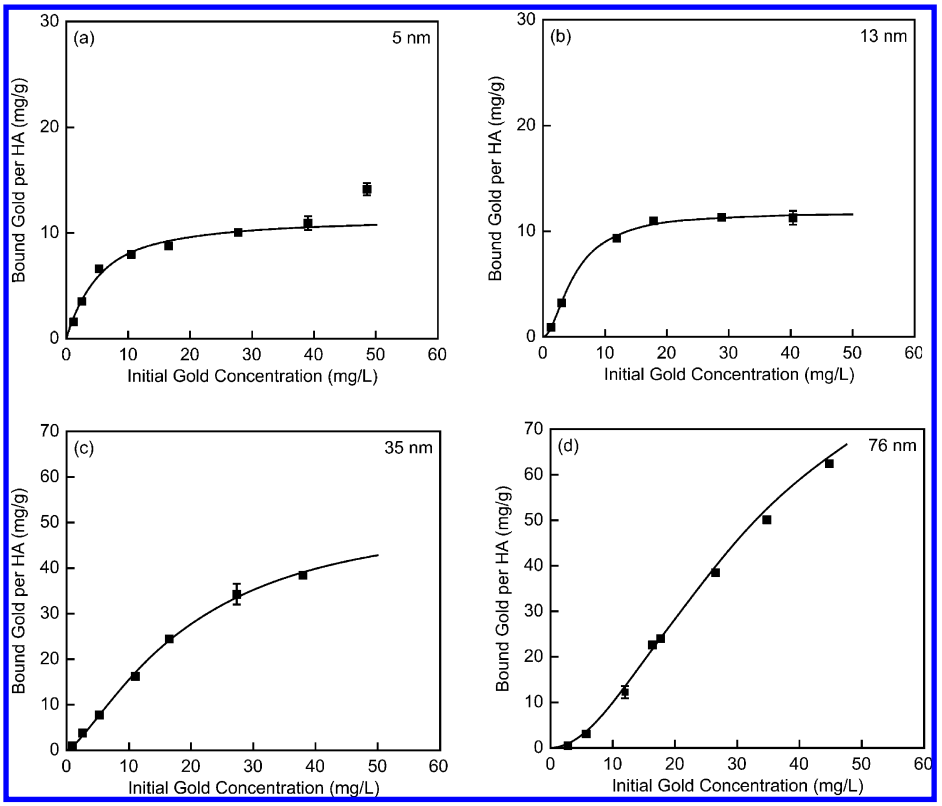

Figure 5. Binding isotherms for bisphosphonate functionalized Au NPs with a mean diameter of (a) 5, (b) 13, (c) 35, and (d) 76 nm adsorbed onto HA crystals in DI water. Note the difference in scale for (a) and (b) versus (c) and (d). Error bars show one standard deviation of the mean (n = 3 per data point). Error bars not shown lie within the data point. Experimental data were modeled by the Langmuir–Freundlich isotherm (eq 2) using nonlinear least-squares regression. Binding constants are reported in Table 2.

Table 2. Binding Constants for 5, 13, 35, and 76 nm Diameter Bisphosphonate Functionalized Au NPs Adsorbed onto HA Crystals Determined by Nonlinear Least-Squares Regression of Langmuir–Freundlich (LF) Isotherms[a]

particle diameter (nm)	K (mg/L)	b	V_{max} (mg/g)	V_{max}* (mg/m^2)	$V_{max}^{\#}$ (#/μm^2)	R^2
5	4.9	1.1	11.7	2.1	1755	0.98
13	5.0	1.7	11.8	2.1	95	0.99
35	19.3	1.4	54.5	9.7	23	0.99
76	33.5	1.8	102.0	18.1	5	1.00

[a] K is the equilibrium Langmuir binding constant, b is the heterogeneity constant, V_{max} is the maximum surface binding (mg Au/g HA), V_{max}* is the maximum surface binding normalized to the specific surface area of HA crystals (mg Au/m^2 HA), $V_{max}^{\#}$ is the maximum number of Au NPs bound per surface area of HA crystals (#/μm^2 HA), and R^2 is the correlation coefficient from the regression.

carboxylate- and phosphonate-functionalized Au NPs despite having ~50% fewer functional groups available for binding due to the greater size of bisphosphonate molecules.[22] The strong binding affinity of bisphosphonate functionalized Au NPs to HA is due to the relative acidity of bisphosphonate groups and the formation of bidentate, possibly even tridentate, ligands with HA.[23,54]

The increased mass of Au NPs bound per HA mass or surface area, V_{max} or V_{max}*, with increased Au NP diameter (Table 2) was driven by a large increase in mass per Au NP with increased Au NP diameter. The increased number of Au NPs bound per HA surface area, $V_{max}^{\#}$, with decreased Au NP diameter (Table 2) was driven by a large increase in the number of NPs at a fixed mass concentration with decreased Au NP diameter. In other words, adsorption of a single larger diameter Au NP provided a substantially greater mass of Au compared to a smaller diameter Au NP, but adsorption of an equal mass of smaller diameter Au NPs provided a substantially greater number of NPs compared to larger diameter Au NPs. The greater surface density of bisphosphonate ligands on larger diameter Au NPs may have also contributed to the increase in V_{max} and V_{max}* with increased Au NP diameter.

The results of this study suggest that for targeted labeling of HA, or calcified tissue, an increased Au NP diameter will improve detection via greater X-ray attenuation due to a greater of mass of gold atoms labeling surfaces (Table 2). A smaller diameter resulted in a greater number of Au NPs labeling HA (Table 2, Figure 4), but X-ray attenuation was shown to be unaffected by surface area and only governed by the mass concentration of Au NPs (Figure 3). Note, however, that this study did not consider deliverability; there was no barrier to transport from the solution to the crystal surface. Smaller Au NPs may be beneficial, if not necessary, for delivery in vivo.

Deliverability of larger nanoparticles to cells or tissues in vivo may be limited by colloidal instability and rapid clearance by the reticuloendothelial system.[30−39] For example, smaller Au NPs (10 nm) achieved improved vascular retention and organ distribution, while larger NPs (50, 100, and 250 nm) were only located within the liver, spleen, and blood, after intravenous injection in rats.[32] Moreover, in vivo delivery to bone tissue requires transport through ~100−400 nm diameter canaliculi with ~40−100 nm available fluid space due to the presence of cellular processes[55,56] and a pericellular matrix that limits diffusion to molecules with an effective diameter less than 10

dx.doi.org/10.1021/cm4035616 | Chem. Mater. 2014, 26, 1187−1194

nm.[57] Therefore, limitations of the Au NP size on delivery will be dependent upon many factors, including the intended application. Intracellular delivery of Au NPs is complex and also dependent on the functional ligands. For example, cellular internalization was shown to be greatest for 50 nm Au NPs compared to smaller or larger Au NPs due to optimal ligand surface density relative to cell surface receptors.[35,36,39] Therefore, the ideal particle diameter for delivery may be highly dependent on the application, including the cells or tissues targeted and required surface functionalization.

CONCLUSIONS

The effects of Au NP size on X-ray attenuation and binding affinity to a targeted surface were investigated for Au NPs exhibiting a mean particle diameter of 5, 13, 35, or 76 nm. The X-ray attenuation of mercaptosuccinic acid functionalized Au NPs and chloroauric acid solutions increased with decreased photon energy and increased linearly with increased gold concentrations ranging 0−50 mM (0−10 g/L) ($p < 0.0001$), but was independent of the particle diameter ($p > 0.85$). Therefore, strategies to improve the X-ray detection of targeted cells and tissues should focus on increasing the mass concentration of delivered nanoparticles. The effects of Au NP size on binding affinity were investigated by measuring binding isotherms for bisphosphonate functionalized Au NPs to hydroxyapatite crystals as a clinically relevant in vitro model for bone mineral or microcalcifications. Decreased Au NP diameter resulted in an increased number but decreased mass of Au NPs adsorbed onto hydroxyapatite crystal surfaces, and thus a lower binding affinity to hydroxyapatite. Adsorption of a single larger diameter Au NP provided a substantially greater mass of Au compared to a smaller diameter Au NP, but adsorption of an equal mass of smaller diameter Au NPs provided a substantially greater number of NPs as compared to larger diameter Au NPs. Therefore, the results of this study suggest that for targeted labeling of hydroxyapatite, or calcified tissue, an increased Au NP diameter will improve detection due to a greater mass of gold labeling surfaces and thus greater X-ray attenuation.

ASSOCIATED CONTENT

Supporting Information

Gold nanoparticle size distributions (PDF). This materials is available free of charge via the Internet at http://pubs.acs.org.

AUTHOR INFORMATION

Corresponding Author

*Phone: (574) 631-7003. E-mail: rroeder@nd.edu.

Present Address

[†]Postdoctoral Research Fellow, Department of Anatomy and Cell Biology, Rush University Medical Center, Chicago, Illinois 60612, United States.

Notes

The authors declare no competing financial interest.

ACKNOWLEDGMENTS

This research was supported by the U.S. Army Medical Research and Materiel Command (W81XWH-06-1-0196) through the Peer Reviewed Medical Research Program (PR054672), and the Walther Cancer Foundation. We acknowledge Timothy L. Conrad for preparing the HA crystals used in binding experiments; the Notre Dame Integrated Imaging Facility (NDIIF) and William Archer for the use of the TEM; and the Notre Dame Center for Environmental Science and Technology (CEST), Suzyanne Guzicki, and Jon Loftus for the use and maintenance of ICP-OES. We thank Dan Meisel and Bruce A. Bunker at Notre Dame for helpful discussions regarding X-ray absorption and scattering processes. J.M.R.T. was supported by a Lindemann Trust Fellowship from the English Speaking Union.

REFERENCES

(1) Yu, S.-B.; Watson, A. D. *Chem. Rev.* **1999**, *99*, 2353−2377.
(2) Hainfeld, J. F.; Slatkin, D. N.; Smilowitz, H. M. *Phys. Med. Biol.* **2004**, *49*, N309−N315.
(3) Hainfeld, J. F.; Slatkin, D. N.; Focella, T. M.; Smilowitz, H. M. *Br. J. Radiol.* **2006**, *79*, 248−253.
(4) Cai, Q.-Y.; Kim, S. H.; Choi, K. S.; Kim, S. Y.; Byun, S. J.; Kim, K. W.; Park, S. H.; Juhng, S. K.; Yoon, K.-H. *Invest. Radiol.* **2007**, *42*, 797−806.
(5) Xu, C.; Tung, G. A.; Sun, S. *Chem. Mater.* **2008**, *20*, 4167−4169.
(6) Jackson, P.; Periasamy, S.; Bansal, V.; Geso, M. *Australas. Phys. Eng. Sci. Med.* **2011**, *34*, 243−249.
(7) Peng, C.; Zheng, L.; Chen, Q.; Shen, M.; Guo, R.; Wang, H.; Cao, X.; Zhang, G.; Shi, X. *Biomaterials* **2012**, *33*, 1107−1119.
(8) Kim, D.; Park, S.; Lee, J. H.; Jeong, Y. Y.; Jon, S. *J. Am. Chem. Soc.* **2007**, *129*, 7661−7665.
(9) Jackson, P. A.; Rahman, W. N. W. A.; Wong, C. J.; Ackerly, T.; Geso, M. *Eur. J. Radiol.* **2010**, *75*, 104−109.
(10) Galper, M. W.; Saung, M. T.; Fuster, V.; Roessl, E.; Thran, A.; Proksa, R.; Fayad, Z. A.; Cormode, D. P. *Invest. Radiol.* **2012**, *47*, 475−481.
(11) Kojima, C.; Umeda, Y.; Ogawa, M.; Harada, A.; Magata, Y.; Kono, K. *Nanotechnology* **2010**, *21*, 245104.
(12) Kattumuri, V.; Katti, K.; Bhaskaran, S.; Boote, E. J.; Casteel, S. W.; Fent, G. M.; Robertson, D. J.; Chandrasekhar, M.; Kannan, R.; Katti, K. V. *Small* **2007**, *3*, 333−341.
(13) Boote, E.; Fent, G.; Kattumuri, V.; Casteel, S.; Katti, K.; Chanda, N.; Kannan, R.; Katti, K.; Churchill, R. *Acad. Radiol.* **2010**, *17*, 410−417.
(14) Alkilany, A. M.; Murphy, C. J. *J. Nanopart. Res.* **2010**, *12*, 2313−2333.
(15) Popovtzer, R.; Agrawal, A.; Kotov, N. A.; Popovtzer, A.; Balter, J.; Carey, T. E.; Kopelman, R. *Nano Lett.* **2008**, *8*, 4593−4596.
(16) Eck, W.; Nicholson, A. I.; Zentgraf, H.; Semmler, W.; Bartling, S. *Nano Lett.* **2010**, *10*, 2318−2322.
(17) Hainfeld, J. F.; O'Connor, M. J.; Bilmanian, F. A.; Slatkin, D. N.; Adams, D. J.; Smilowitz, H. M. *Br. J. Radiol.* **2011**, *84*, 526−533.
(18) Chanda, N.; Kattumuri, V.; Shukla, R.; Zambre, A.; Katti, K.; Upendran, A.; Kulkami, R. R.; Kan, P.; Fent, G. M.; Casteel, S. W.; Smith, C. J.; Boote, E.; Robertson, J. D.; Cutler, C.; Lever, J. R.; Katti, K. V.; Kannan, R. *Proc. Natl. Acad. Sci. U.S.A.* **2010**, *107*, 8760−8765.
(19) Kim, D.; Jeong, Y. Y.; Jon, S. A. *ACS Nano* **2010**, *4*, 3689−3696.
(20) Aydogan, B.; Li, J.; Rajh, T.; Chaudhary, A.; Chmura, S. J.; Pelizzari, C.; Wietholt, C.; Kurtoglu, M.; Redmond, P. *Mol. Imaging Biol.* **2010**, *12*, 463−467.
(21) Zhang, Z.; Ross, R. D.; Roeder, R. K. *Nanoscale* **2010**, *2*, 582−586.
(22) Ross, R. D.; Roeder, R. K. *J. Biomed. Mater. Res.* **2011**, *99A*, 58−66.
(23) Ross, R. D.; Cole, L. E.; Roeder, R. K. *J. Nanopart. Res.* **2012**, *14*, 1175 (11 pp).
(24) Cole, L. E.; Vargo-Gogola, T. C.; Roeder, R. K. *Biomaterials* **2014**, *35*, 2312−2321.
(25) Debouttière, P.-J.; Roux, S.; Vocanson, F.; Billotey, C.; Beuf, O.; Favre-Réguillon, A.; Lin, Y.; Pellet-Rostaing, S.; Lamartine, R.; Perriat, P.; Tillement, O. *Adv. Funct. Mater.* **2006**, *16*, 2330−2339.
(26) Alric, C.; Taleb, J.; Duc, G. L.; Mandon, C.; Billotey, C.; Meur-Herland, A. L.; Brochard, T.; Vocanson, F.; Janier, M.; Perriat, P.; Roux, S.; Tillement, O. *J. Am. Chem. Soc.* **2008**, *130*, 5908−5915.

(27) Link, S.; El-Sayed, M. A. *J. Phys. Chem. B* **1999**, *103*, 4212−4217.
(28) Lee, K.-S.; El-Sayed, M. A. *J. Phys. Chem. B* **2006**, *110*, 19220−19225.
(29) Jain, P. K.; Lee, K. S.; El-Sayed, I. H.; El-Sayed, M. A. *J. Phys. Chem. B* **2006**, *110*, 7238−7248.
(30) Liu, Y.; Shipton, M. K.; Ryan, J.; Kaufman, E. D.; Franzen, S.; Feldheim, D. L. *Anal. Chem.* **2007**, *79*, 2221−2229.
(31) Zhang, G.; Yang, Z.; Lu, W.; Zhang, R.; Huang, Q.; Tian, M.; Liang, D.; Li, C. *Biomaterials* **2009**, *30*, 1928−1936.
(32) De Jong, W. H.; Hagens, W. I.; Krystek, P.; Burger, M. C.; Sips, A. J. A. M.; Geertsma, R. E. *Biomaterials* **2008**, *29*, 1912−1919.
(33) Sonavane, G.; Tomoda, K.; Makino, K. *Colloids Surf., B* **2008**, *66*, 274−280.
(34) Perrault, S. D.; Walkey, C.; Jennings, T.; Fischer, H. C.; Chan, W. C. W. *Nano Lett.* **2009**, *9*, 1909−1915.
(35) Chithrani, B. D.; Ghazani, A. A.; Chan, W. C. W. *Nano Lett.* **2006**, *6*, 662−668.
(36) Jiang, W.; Kim, B. Y. S.; Rutka, J. T.; Chan, W. C. W. *Nat. Nanotechnol.* **2008**, *3*, 145−150.
(37) Cho, E. C.; Au, L.; Zhang, Q.; Xio, Y. *Small* **2010**, *6*, 517−522.
(38) Oh, E.; Delehanty, J. B.; Sapsford, K. E.; Susumu, K.; Goswami, R.; Blanco-Canosa, J. B.; Dawson, P. E.; Granek, J.; Shoff, M.; Zhang, Q.; Goering, P. L.; Huston, A.; Medintz, I. L. *ACS Nano* **2011**, *5*, 6434−6448.
(39) Albanase, A.; Tang, P. S.; Chan, W. C. W. *Annu. Rev. Biomed. Eng.* **2012**, *14*, 1−16.
(40) Frens, G. *Colloid Polym. Sci.* **1972**, *250*, 736−741.
(41) Slot, J. W.; Geuze, H. J. *Eur. J. Cell Biol.* **1985**, *38*, 87−93.
(42) Elzey, S.; Tsai, D.-H.; Rabb, S. A.; Yu, L. L.; Winchester, M. R.; Hackley, V. A. *Anal. Bioanal. Chem.* **2012**, *403*, 145−149.
(43) Roeder, R. K.; Converse, G. L.; Leng, H.; Yue, W. *J. Am. Ceram. Soc.* **2006**, *89*, 2096−2104.
(44) Kinniburgh, D. G. *Environ. Sci. Technol.* **1986**, *20*, 895−904.
(45) Kimling, J.; Maier, M.; Okenve, B.; Kotaidis, V.; Ballot, H.; Plech, A. *J. Phys. Chem. B* **2006**, *110*, 15700−15707.
(46) Henglein, A.; Giersig, M. *J. Phys. Chem. B* **1999**, *103*, 9533−9539.
(47) Mei, B. C.; Oh, E.; Susumu, K.; Farrell, D.; Mountziaris, T. J.; Mattoussi, H. *Langmuir* **2009**, *25*, 10604−10611.
(48) Berger, M. J.; Hubbell, J. H.; Seltzer, S. M.; Chang, J.; Coursey, J. S.; Sukumar, R.; Zucker, D. S.; Olsen, K. *XCOM: Photon Cross Section Database*; National Institute of Standards and Technology: Gaithersburg, MD, 2010; available at http://physics.nist.gov/xcom.
(49) Hubbell, J. H.; Seltzer, S. M. *Table of X-ray Mass Attenuation Coefficients and Mass Energy-Absorption Coefficients (version 1.4)*; National Institute of Standards and Technology: Gaithersburg, MD, 2004; available at http://physics.nist.gov/xaamdi.
(50) Hubbell, J. H.; Gimm, H. A.; Overbo, I. *J. Phys. Chem. Ref. Data* **1980**, *9*, 1023−1147.
(51) Hubbell, J. H. *Natl. Stand. Ref. Data Ser.* **1969**, *29*, 85pp.
(52) Ricker, A.; Liu-Snyder, P.; Webster, T. J. *Int. J. Nanomed.* **2008**, *3*, 125−132.
(53) Meagher, M. J.; Leone, B.; Turnbull, T. L.; Ross, R. D.; Zhang, Z.; Roeder, R. K. *J. Nanopart. Res.* **2013**, *15*, 2146 (10pp).
(54) Nancollas, G. H.; Tang, R.; Phipps, R. J.; Henneman, Z.; Gulde, S.; Wu, W.; Mangood, A.; Russell, R. G. G.; Ebetino, F. H. *Bone* **2006**, *38*, 617−627.
(55) Knothe-Tate, M. L.; Niederer, P.; Knothe, U. *Bone* **1998**, *22*, 107−117.
(56) You, L.-D.; Weinbaum, S.; Cowin, S. C.; Schaffler, M. B. *Anat. Rec.* **2004**, *278A*, 505−513.
(57) Wang, L.; Ciani, C.; Doty, S. B.; Fritton, S. P. *Bone* **2004**, *34*, 499−509.